Computational Materials Science 96 (2015) 559–566

Contents lists available at ScienceDirect

Computational Materials Science

journal homepage: www.elsevier.com/locate/commatsci

Modeling microtubule cytoskeleton via an active liquid crystal elastomer model

Houfu Fan, Shaofan Li *

Department of Civil and Environmental Engineering, University of California, Berkeley, CA 94720, USA

ARTICLE INFO

Article history:
Received 8 March 2014
Accepted 20 April 2014
Available online 3 July 2014

Keywords:
Biopolymer
Cytoskeleton
Liquid crystal elastomer
Microtubule
Soft matter

ABSTRACT

In this work, a three-dimensional (3D) liquid crystal polymer model is developed to model the microtubule cytoskeleton aggregate and to study its interaction with the extracellular matrix. In the proposed microtubule cytoskeleton model, the cytoskeleton aggregate is treated as a homogenized liquid crystal elastomer medium, with an extra active stress term included to account for the effect of the active process of Guanosine Triphosphate (GTP) hydrolysis. The cell extracellular matrix (ECM) is modeled as a hyperelastic material. The specific and non-specific interactions between the cell and its ECM are modeled by a Coarse-Grained Contact Model. Surface tension effects are incorporated into the simulation, through a Multiscale Dynamic Wetting Model, to account for the interface conditions between the cell and its surrounding environment. The cell model is implemented in a Lagrange type Galerkin formulation. The numerical results show that the cell can sense and move under the gradient of matrix elasticity.

1. Introduction

From structure point of view, a cell consists of cell membrane, cell cytoskeleton and cell nuclei. The cytoskeleton is the cell's scaffold, which mainly composes of actin-filaments, intermediate filaments, and microtubules. To model such a complex system as a whole at micro-meter scale, continuum modeling is the best approach, due to its distinct advantages in providing the most direct and relevant information on bio-physical and physiologically state of the cell. It has become a general consensus now in the biophysics community that the actin filament is essentially an active nematic gel, e.g. [13–15,37], and various liquid-crystal like nematic gel hydrodynamics models [35,36] have been proposed in the simulation of cells. On the other hand, there is a lack of modeling effort in studying intermediate filaments and microtubules, which are not only important biomolecular polymers inside the cell, but also the main cytoskeleton structure components that provide elastic stiffness and help force transferring.

In recent years, there are several cell rigidity sensing models that have been proposed, such as Two-spring rigidity sensing model [25], Non-linear elasticity of the Extracellular Matrix (ECM)/Cell interaction model [31], Stress-fiber polarization model [34] and a mechano-sensing and force generation model in contractile cells [26]. These are very successful models with biology insights, and most of these models are one-dimensional or two-dimensional elasticity models. The contributors of these cell elasticity theories are from diverse fields: physics or bio-physics, materials science, chemistry, and applied mechanics. To the best of the author's knowledge, there are very few or even no three dimensional cell model that can simulate a cell interacting with its ECM in a continuum approach. It is the intent of this work to propose a soft matter cell model to simulate the contact/adhesion of cell on the ECM and hence cell spreading/crawling on a stiffness varying substrate.

The main novelty and distinction of the present work is that it combines the proposed active soft matter model, together with the lately developed Coarse-Grained Contact Model [22–24], and the Multiscale Dynamic Wetting Model [19] to successfully simulates cell contact/adhesion/crawling upon different elastic substrate.

This paper is organized into five Sections. The constitutive models of cell and the extracellular matrix are discussed in Section 2. In Section 3, the Coarse-Grained Contact Model and the Multiscale Dynamic Wetting Model are briefly reviewed. In Section 4, a few numerical examples are presented, focusing on their relevance to cellular biology applications. Finally, in Section 5, we close our presentation by making a few remarks.

2. Mesoscale continuum modeling of cell and ECM

2.1. Active stress based liquid crystal elastomer model

Liquid crystals have biphasic properties by exhibiting both liquid and solid characteristics. For instance, a liquid crystal may

* Corresponding author. Tel.: +1 5106425362; fax: +1 5106438928.
E-mail address: shaofan@berkeley.edu (S. Li).

http://dx.doi.org/10.1016/j.commatsci.2014.04.041
0927-0256/

be fluid similar to a liquid with vanishing shear modulus, while having a long range orientational order and therefore a strain gradient elasticity associated with deformations of the order parameter. Many biological materials contain liquid crystalline phase, and the most common examples are cell membranes, phospholipid,cholesterol, DNA, various proteins, among others (see [32]).

Actin cytoskeleton filaments have polarity, and actin monomers orient with their cleft towards the pointed or the minus end and their head towards to the barbed or plus end. Under suitable physiological conditions, G-actin monomer may be transformed to F-actin (polymer form) by ATP at the plus end, which is called polymerization, and it may be depolymerized at the minus end. For mesoscale modeling, we may assign a unit vector at each material point, hence a continuous director field may be established to represent local polarization of a homogenized actin filament/cytoplasm representative volume element (RVE). This is the bio-physics foundation or justification for developing a nematic fluid hydrodynamics to model a polar actin filament/cytoplasm gel at mesoscale level. The local orientation of this director field is central to many cellular processes such as cell motility and locomotion, cell adhesion, and cell division.

Although liquid crystal behaviors of cytoskeleton filaments were discovered in late 1990s and early e.g. [27,28], it is not until recently that people have started to model actin cytoskeleton motion or lamellipodium motion by using nematic liquid crystal hydrodynamics [15,13,12].

However, the actin filament is only responsible for cytosis process, while microtubules make mitosis and cell locomotion possible, because it provides most strength and structure support in cytoskeletons. The microtubule is the main component of cytoskeleton, and it has a hollow, cylindrical structure assembled by polymerization of α/β dimers of tubulin. Microtubules have a distinct polarity or lattice structure that is important for their biological function. Tubulin polymerizes end to end with an α subunit of one tubulin dimer connecting with a β subunit of the next. We refer the end terminated by the α-subunit as the minus end, and the end terminated by the β-subunit as the plus end. In vitro, purified tubulin polymerizes more quickly from the plus end, while slowly growing at the minus end. In essence, the microtubule is a bio-polymer with crystal structure, or in short a liquid crystal elastomer.

Moreover, microtubule assemblies are highly dynamic, and they frequently grow and shrink at a rapid yet constant rate at the plus end, which is known as 'dynamic instability'. During polymerization, both the α- and β-subunits of the tubulin dimer are bound to a molecule of GTP. While the GTP bound to α-tubulin is stable, the GTP bound to β-tubulin may be hydrolyzed to GDP shortly after assembly. The kinetics of GDP-tubulin are different from those of GTP-tubulin; GDP-tubulin is prone to depolymerization. A GDP-bound tubulin subunit at the tip of a microtubule will fall off, though a GDP-bound tubulin in the middle of a microtubule cannot spontaneously pop out. The main factor dictates whether microtubules grow or shrink is the rate of GTP hydrolysis. At high free GTP-tubulin dimer concentrations, hydrolysis is outpaced by rapid assembly at the plus end, thereby forming a rigid GTP-cap, whereas concerted GTP hydrolysis at the plus end will cause protofilaments rapidly disassemble. Once assembled, polarized arrays of microtubules provide tracks for the transport of organelles and chromosomes. This transport is driven by the motor proteins such as kinesin and dynein that interact with and move along the lateral surface of the microtubule. Motor proteins are molecular machines, and they convert chemical energy derived from ATP hydrolysis into mechanical work used for cellular motility.

At mesoscale or macroscale level, if one assigns a crystal lattice structure to an entropic elastomer, one will end up with a soft matter material – *the liquid crystal elastomer*! Liquid crystal elastomers or polymers consist of networks of cross-linked polymeric chains, each of which contains rigid rod-like molecules called mesogens with long range structure order e.g. [29,30]. Liquid crystal elastomers combine the elastic properties of polymers with the order inherent in nematic liquid crystals. Liquid crystal elastomer has an interesting property: Stretching a monodomain strip of nematic elastomer in a direction transverse to the nematic director will result in an energy-free rotation of the director, giving rise to a soft elastic response [8].

In this work, we propose in the first time to use a liquid crystal elastomer-like constitutive relation to model microtubule bundles or aggregates (see Fig. 1).

In fact the cell is a living object, the conventional passive liquid crystal hydrodynamics is insufficient to model many important features of a living cell, because the free-energy based soft matter approach may not be valid, and it is intended for systems at equilibrium states. In this work, like the modeling of actin filament e.g. [4], we postulate that the Cauchy stress inside the microtubule aggregated may be divided into two parts: $\boldsymbol{\sigma} = \boldsymbol{\sigma}^p + \boldsymbol{\sigma}^a$, in which, $\boldsymbol{\sigma}^a$ is the an active stress expressed as,

$$\boldsymbol{\sigma}^a = -\zeta \mathbf{h} \otimes \mathbf{h}, \tag{1}$$

which accounts for the force generated along the direction of the local director field $\mathbf{h}$; ζ is an activity constant that is related to the chemical energy release rate of the GTP inside the cell.

In order to get the passive part of the stress, we adopted the following free energy density of the liquid crystal elastomer [8],

$$\mathcal{F} = \frac{\mu}{2}\left[|\mathbf{F}|^2 - \frac{s-1}{s}\left|\mathbf{F}^T\mathbf{h}\right|^2 + (s-1)|\mathbf{F}\mathbf{h}_0|^2 - \frac{(s-1)^2}{s}\left(\mathbf{F}^T\mathbf{h}\cdot\mathbf{h}_0\right)^2 - 3\right] + J\frac{\kappa(s-1)^2}{2s}|\mathbf{F}^T\mathbf{G}|^2, \tag{2}$$

where $\mathbf{F}$ is the deformation gradient, and J is its determinant, i.e.

$$\mathbf{F} = \frac{\partial \mathbf{x}}{\partial \mathbf{X}}, \text{ and } J = \det|\mathbf{F}|,$$

where $\mathbf{x}$ is the position vector of a material point at the current configuration that is defined as

$$\mathbf{x} = \mathbf{X} + \mathbf{u},$$

where $\mathbf{u}(\mathbf{X})$ is the displacement field, and $\mathbf{X}$ is the position vector of the material point at the reference or material configuration.

The corresponding passive part of the first Piola–Kirchhoff stress part can be obtained by,

$$\begin{aligned}\mathbf{P}^p &= \frac{\partial \mathcal{F}}{\partial \mathbf{F}} \\ &= \mu\left[\mathbf{F} - \frac{s-1}{s}\mathbf{h}\otimes(\mathbf{h}\cdot\mathbf{F}) + (s-1)(\mathbf{F}\mathbf{h}^0)\otimes\mathbf{h}^0 - \frac{(s-1)^2}{s}(\mathbf{h}\cdot\mathbf{F}\mathbf{h}^0)(\mathbf{h}\otimes\mathbf{h}^0)\right] \\ &\quad + \frac{\kappa(s-1)^2}{s}J\mathbf{G}\mathbf{G}^T\mathbf{F}^{-T} - p\mathbf{F}^{-T},\end{aligned} \tag{3}$$

which can be converted to the Cauchy stress as,

$$\begin{aligned}\boldsymbol{\sigma}^p &= \frac{1}{J}\mathbf{P}^p\cdot\mathbf{F}^T \\ &= \frac{\mu}{J}\left[\mathbf{C} - \frac{s-1}{s}\mathbf{h}\otimes(\mathbf{h}\cdot\mathbf{F}) + (s-1)\mathbf{F}\mathbf{h}^0\otimes(\mathbf{F}\mathbf{h}^0) - \frac{(s-1)^2}{s}(\mathbf{h}\cdot\mathbf{F}\mathbf{h}^0)(\mathbf{h}\otimes\mathbf{F}\mathbf{h}^0)\right] \\ &\quad + \frac{\kappa(s-1)^2}{s}\mathbf{G}\mathbf{G}^T - \frac{p}{J}\mathbf{I},\end{aligned} \tag{4}$$

where the μ is the shear modulus, κ is the Frank modulus, s is the step length anisotropy, $\mathbf{C} = \mathbf{F}^T\mathbf{F}$ is the Right Cauchy–Green tensor, $\mathbf{G} = \nabla_{\mathbf{x}} \otimes \mathbf{h}$ is the gradient of the director field, $\mathbf{h}$ and $\mathbf{h}^0$ represents

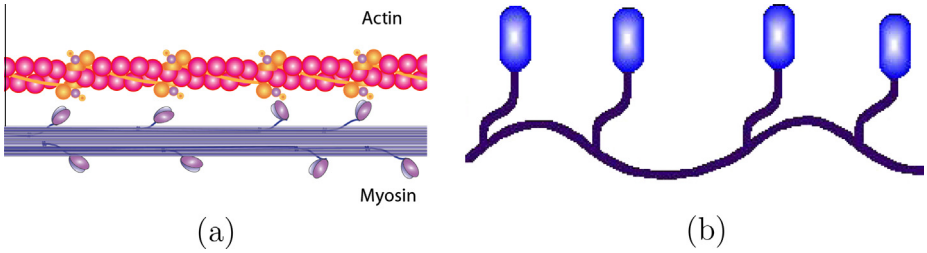

Fig. 1. Comparison between (a) microdomains of Non-muscle Myosin II (NM II) and (b) mesogens in liquid crystal elastomers.

the director field in the current and reference configuration, respectively.

In addition to the displacement field $\mathbf{u}$, the Cauchy stress for the active liquid crystal elastomer is also dependent on the director field $\mathbf{h}$. In order to find the director field of liquid crystal elastomer, an additional equation for the director field $\mathbf{h}$ is needed. In the proposed microtubule cytoskeleton model, the evolution of the director field $\mathbf{h}$ is obtained by adopting the following Allen–Cahn approach [3],

$$\frac{D\tilde{\mathbf{h}}}{Dt} = -\mathcal{L}\frac{\delta \mathcal{F}}{\delta \mathbf{h}}, \tag{5}$$

where $\mathcal{L}$ is a material tensor parameter, which characterizes the diffusivity or transport property of microtubules. With some manipulations, one may arrive at the following governing equation for the director field $\mathbf{h}$,

$$\frac{D\tilde{\mathbf{h}}}{Dt} = \mu\mathcal{L}\left[\frac{s-1}{s}\mathbf{h}\mathbf{F}\mathbf{F}^T + \frac{(s-1)^2}{s}(\mathbf{h}\cdot\mathbf{F}\mathbf{h})\left(\mathbf{F}\mathbf{h}^0\right)\right] + \frac{\kappa(s-1)^2}{s}\mathcal{L}\cdot\nabla\left[\mathbf{F}^{-1}J(\mathbf{F}^{-T}\mathbf{G})\right]. \tag{6}$$

One may note that in Eq. (6), a corotational convected objective time rate $\frac{D\mathbf{h}}{Dt}$ is used, which is very important for large deformations dynamic computations. In this work, it is chosen as

$$\frac{D\tilde{\mathbf{h}}}{Dt} = \frac{D\mathbf{h}}{Dt} + \frac{1}{2}(\ell^T\mathbf{h} - \boldsymbol{\omega}\mathbf{h}), \tag{7}$$

where $\ell = \dot{\mathbf{F}}\mathbf{F}^{-1}$ is the velocity gradient and $\boldsymbol{\omega} = \frac{1}{2}(\ell - \ell^T)$ is the spin tensor.

The displacement (essential) boundary condition for the director field is prescribed all over cell surface during the entire simulation process. That is,

$$\mathbf{h} = \mathbf{h_0} = \mathbf{n}, \ \forall \mathbf{x} \in \partial\Omega_1, \tag{8}$$

where $\mathbf{h_0}$ is the initial director field and $\mathbf{n}$ is the current unit out-normal on the cell surface at each material point. The reasons why we choose the such initial director field and essential boundary condition are the following. The orientation the lipid bilayer membrane is always along the normal direction of cell surface, which may be viewed as an ideal smectic A phase of liquid crystal. In the original undeformed configuration, the direction of lipid bilayer is along the radial direction. Thus, it may be a natural choice of boundary condition and initial condition that the stress fibers have the same orientation as that of the lipid bilayer at the boundary, and it is naturally to assume the interior stress fiber being as a continuation of lipid bilayer from surface to interior.

2.2. Hyperelastic model

Hyperelastic material models have been used a lot in cell modeling. There are many Hyperelastic models for rubber-like materials in the literature, a comparison of different Hyperelastic models can be found in [18]. In this research, the modified Mooney–Rivlin material [7] is chosen to model the cell ECM. The strain energy density function W for the modified Mooney–Rivlin material is,

$$W = c_1(I_1 - 3I_3^{1/3}) + c_2(I_2 - 3I_3^{2/3}) + \frac{1}{2}\lambda(\ln I_3)^2, \tag{9}$$

where c_1, c_2 and λ are material constants. I_1, I_2 and I_3 are three invariants of the right Cauchy–Green tensor $\mathbf{C} = \mathbf{F}^T\mathbf{F}$, given as follows,

$$I_1 = \mathrm{tr}(\mathbf{C}), \quad I_2 = \frac{1}{2}\left[(\mathrm{tr}(\mathbf{C}))^2 - \mathbf{C}^2\right], \quad I_3 = \det(\mathbf{C}). \tag{10}$$

The corresponding constitutive relations can be expressed in terms of the second Piola–Kirchhoff stress tensor $\mathbf{S} = S_{IJ}\mathbf{E}_I \otimes \mathbf{E}_J$, and the invariants of the right Cauchy–Green tensor,

$$\mathbf{S} = 2\left\{(c_1 + c_2 I_1)\mathbf{I} - c_2\mathbf{C} - (c_1 I_3^{1/3} + 2c_2 I_3^{2/3} - \lambda \ln I_3)\mathbf{C}^{-1}\right\}. \tag{11}$$

3. Cell interactions with the environment

3.1. Coarse-Grained Contact Model

The ability to send and receive signals is essential to the survival of a cell. In fact, all cells rely on cell signaling to detect and respond to cues in their environment. In stead of trying to simulate of the whole picture of cell signaling, here we are particularly interested in the way a cell adheres or responds to the rigidity of the ECM. A cell interacts with the extracellular matrix through specific and non-specific bonded forces [1,2,21]. For simplicity, we do not differentiate the two in the present case. From microscale perspectives, this interactions originate from intermolecular interactions among different bodies. In our simulation, the body–body interaction between the cell and the ECM are modeled by the recently developed Coarse-Grained Contact Model [22–24]. This adhesive contact model is very useful in the simulations of soft matter adhesion contact in mesoscale level. In comparison to classical contact algorithms, which usually treat the bodies as rigid, or at least very stiff solids, CGCM can deal with the adhesive contact between two soft bodies with extremely large deformation. The key technical ingredient of CGCM is to introduce an adhesive contact potential of the two bodies, based on the homogenization of molecular interaction between individual atoms or molecules. The kinematic description of two interacting bodies is shown in Fig. 2. Consider the interaction of two distinct bodies at the current configurations Ω_1 and Ω_2. The total potential energy of the system can be written as,

$$\Pi = \sum_{I=1}^{2}(\Pi_{int,I} - \Pi_{ext,I} + \Pi_{AC}), \tag{12}$$

where $\Pi_{int,I}$ and $\Pi_{ext,I}$ are the internal energy and external energy for body $\Omega_I, I = 1, 2$. Π_{AC} denotes the homogenized interaction energy due to the interbody adhesive contact. From microscale

perspectives, the internal energy $\Pi_{int,I}$ can be viewed as the particle interactions within the two bodies. The cellular intrabody interactions are mainly due to covalent bonds and ionic bonds, which are predominant in short range. On the contrary, Π_{AC} comes from the interbody interactions. The cellular interbody interactions are mainly attributed to covalent and van der Waals interactions, which is long range and in general much weaker than the covalent bond force. In this work, we only model the cellular interbody interaction as the van der Waals interaction, and such simplified approximation has been adopted by some researchers e.g. [21].

Suppose that there are two atoms located at $\mathbf{x}_1$ and $\mathbf{x}_2$ interacting with each other via an interatomic potential ϕ, which is a function of the current bond length $r := |\mathbf{x}_1 - \mathbf{x}_2|$. $\phi(r)$ can be any potential that is suitable for the specific physical bonding. There are several elementary interaction potentials to describe long range interbody interactions. In this work, the 12-6 Lennard-Jones potential is adopted, i.e,

$$\phi(r) = \epsilon\left(\frac{\sigma_0}{r}\right)^{12} - 2\epsilon\left(\frac{\sigma_0}{r}\right)^{6}, \tag{13}$$

where ϵ is the potential well (in the unit of energy) and σ_0 is the equilibrium distance. Summing up all the inter-body interactions between atoms in the two bodies, one may arrive at the final form of the homogenized interaction energy for the adhesive contact,

$$\Pi_{AC} = \int_{\Omega_1}\int_{\Omega_2} \beta_1\beta_2\phi(r)dv_2dv_1, \quad r = |\mathbf{x_1} - \mathbf{x_2}|, \tag{14}$$

where β_1 and β_2 represent the current particle densities located at points $\mathbf{x_1} \in \Omega_1$ and $\mathbf{x_2} \in \Omega_2$. Take the first variation of the homogenized interaction energy Π_{AC} ,

$$\begin{aligned}\delta\Pi_{AC} &= \int_{\Omega_1}\int_{\Omega_2} \beta_1\beta_2\left(\frac{\partial\phi(r)}{\partial\mathbf{x}_1}\cdot\delta\mathbf{u}_1 + \frac{\partial\phi(r)}{\partial\mathbf{x}_2}\cdot\delta\mathbf{u}_2\right)dv_1dv_2 \\ &= -\int_{\Omega_1}\beta_1\mathbf{b}_1\cdot\delta\mathbf{u}_1dv_1 - \int_{\Omega_2}\beta_2\mathbf{b}_2\cdot\delta\mathbf{u}_2dv_2,\end{aligned}$$

where the body forces are defined as

$$\mathbf{b}_1(\mathbf{x}_1) := -\frac{\partial\Phi_2}{\partial\mathbf{x}_1}, \quad \Phi_2 := \int_{\Omega_2}\beta_2\phi(r)dv_2;$$

$$\mathbf{b}_2(\mathbf{x}_2) := -\frac{\partial\Phi_1}{\partial\mathbf{x}_2}, \quad \Phi_1 := \int_{\Omega_1}\beta_1\phi(r)dv_1.$$

For the detailed information on the theory as well as computational formulations of the Coarse-Grained Contact Model, the reader may consult to [22–24], except that the adhesive energy constant ϵ used here is dependent on substrate elasticity.

3.2. Multiscale dynamic wetting model

In order to start crawling on the ECM, a cell has to first be able to adhere on it. Like droplet wetting on a surface, cell spreading process is facilitated by the interface surface tension effects [6].

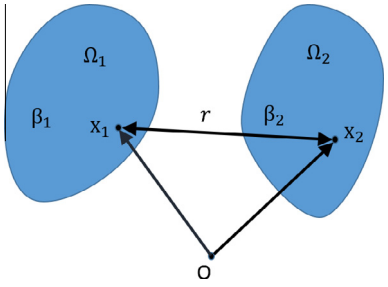

Fig. 2. The kinematics of two interacting bodies.

In this work, the recently developed multiscale dynamics wetting model [19] is used.

The MDWM is a model that combines the conventional hydrodynamic moving contact line theory and a modified Gurtin–Murdoch surface elasticity theory [9,10] with the CGCM, such that a droplet is levitated above the solid substrate, which completely eliminates the singularity problem of conventional hydrodynamics contact line theory.

In addition to the conventional equations of motion for the bulk, the MDWM consider a set of surface equilibrium equations along different interphases,

$$\nabla_s\cdot\boldsymbol{\varsigma}_\alpha + \mathbf{t}_\alpha = \rho_{s\alpha}\mathbf{a}_\alpha, \quad \alpha = G, L, S, \tag{15}$$

where $\alpha = G, L, S$ denotes for gas (G), liquid (L), and solid (S) phases, respectively. $\rho_{s\alpha}$ is the surface mass density, $\boldsymbol{\varsigma}_\alpha$ is the surface stress, $\mathbf{t}_\alpha$ is traction vector, and $\mathbf{a}_\alpha$ is the mass material acceleration. ∇_s is the surface gradient operator that is defined as

$$\nabla_s := \nabla - \mathbf{n}(\mathbf{n}\cdot\nabla), \tag{16}$$

where $\mathbf{n}$ is the unit out-normal of the surface. Applying the Galerkin weakform formulation to the surface equilibrium equations, one may get the resultant force applied on the liquid surface,

$$\mathbf{F}_L^{srf} = -\sum_{I_s=1}^{N_{Snode}}\left\{\int_{\Gamma_{LS}}\frac{\partial N_{I_s}}{\partial\mathbf{x}}:\boldsymbol{\varsigma}_{LS}ds + \int_{\Gamma_{LG}}\frac{\partial N_{I_s}}{\partial\mathbf{x}}:\boldsymbol{\varsigma}_{LG}ds + \int_{\Gamma_{SG}}\frac{\partial N_{I_s}}{\partial\mathbf{x}}:\boldsymbol{\varsigma}_{SG}ds\right\}, \tag{17}$$

where N_{Snode} is the number of nodes on the liquid surface, Γ_{LS}, Γ_{LG} and Γ_{SG} are the three interfaces.

4. Modelings and simulations

In this section, we present three modeling and simulation examples that are employing the proposed liquid crystal polymer cell model to study deformation of cells and their interaction with the environment. First, to validate the soft matter based cell model, we employ the proposed the cell model to simulate the deformation of a thin crystal polymer shell to mimic the deformation of the red blood cell, and we compare our results with the simulation obtained by using Helfrich's cell membrane model [11]. Then we use the proposed soft matter cell model together with the Coarse-Grained Contact Model (CGCM) and multiscale dynamic wetting model (MDWM) to simulate its contact/adhesion with the substrate of a uniform elastic constant. At last, we present a simulation of the interaction between a liquid crystal elastomer droplet and an elastic stiffness varying substrate to explore cell crawling phenomenon.

4.1. Model verification: simulation of biconcave shape of red blood cells

A validation problem for Helfrich's cell membrane model [11] is to simulate the shape of red blood cells, and the Helfrich model successfully captured the biconcave shape of red blood cells. To validate the proposed liquid crystal elastomer model, in this example, we construct a thin liquid crystal elastomer vesicular shell to represent a red blood cell membrane structure, and watch it to deform until reaching to its equilibrium state. Just as that of the Helfrich model, the simulation result shows that the proposed model can also replicate the biconcave cell shape of the red blood cell as shown in Fig. 3. Moreover, we would like to point out that the Helfrich model is a membrane model that has no intrinsic thickness, whereas the thickness of a typical red blood cell is ranging from 0.5 μm to 2.5 μm. The thickness of the presented liquid crystal elastomer shell is set about 0.3 μm, and we believe that

similar simulations would work for thickness up to 2 μm for a 10 μm diameter cell.

An open cross section of the initial shape of the hollow cell is shown in Fig. 3(a). The dimension of the cell model is $R(radius) \times H(height) \times T(thickness) = 5\ \mu m \times 3\ \mu m \times 0.5\ \mu m$. The initial director field is prescribed along the surface normal direction of the outer surface.

The density of the liquid crystal elastomer is chosen as $\rho^0 = 1.0 \times 10^3\ kg/m^3$. The following material properties and constants are used in the simulation: the shear modulus $\mu = 1.0 \times 10^4\ N/m^2$, the Frank modulus $\kappa = 1.0 \times 10^{-11}$ N, the step length anisotropy $s = 2.0$.

In this simulation, the RKPM meshfree particle method [17,16] is used. A total of 30,728 particles are used in the meshfree discretization of the hollow cell. As shown in Fig. 3(b), during the simulation, the hollow cell eventually relaxes into a biconcave cell membrane shape.

4.2. 3D cell contact/adhesion with an elastic substrate

In the following simulation example, the cell is modeled as a three-dimensional (3D) solid sphere or droplet, which is initially in the referential configuration, with a radius of $r = 5$ μm. A schematic illustration of the cell-substrate adhesive contact model is shown in Fig. 4. The elastic substrate is modeled as a 3D rectangular block with a dimension of ($a \times a \times H = 37.5\ \mu m \times 37.5\ \mu m \times 4.5\ \mu m$). In the finite element analysis model, the finite element mesh of the cell consists of 10,976 elements and 11,621 nodes, and the mesh of the substrate consists of 2700 elements and 3844 nodes. The density of the cell is chosen as $\rho^0 = 1.0 \times 10^3\ kg/m^3$, and the other material properties and constants are: the shear modulus $\mu = 1.0 \times 10^4\ N/m^2$, the Frank modulus $\kappa = 1.0 \times 10^{-11}$ N, the step length anisotropy $s = 2.0$.

In this study, the ECM is modeled as a Hyperelastic material of Mooney–Rivlin type. The initial density is $\rho^0 = 1.0 \times 10^3\ kg/m^3$, and the material constants are $c_1 = 2.126 \times 10^3$ Pa, $c_2 = 1.700 \times 10^2$ Pa and $\lambda = 1.700 \times 10^5$ Pa. Before the starting point of the simulation, the cell is kept still, and it is in a suspension state. The cell is released at the start of the computation. The initial gap between the lowest point of the cell and substrate is set at 200 nm, and the bottom surface of the substrate is fixed during entire simulation period. Essential boundary condition for the director field is prescribed all over the cell surface, i.e, pointing along the current unit out-surface normal. A time sequence of a cell contact/adhesion over the homogeneous deformable substrate is shown in Fig. 5. The color contour is the effective stress contour, and the cygan arrow represents the director field. One can easily see the 3D elastic cell–substrate contact/adhesion process, This simulation process proves that the present cell model is actually capable of stably adhering to the substrate, with the help of the Coarse-Grained Contact Model. In addition, the pure 3D simulation provides a convenient way to capture the cell morphology changes described in [20].

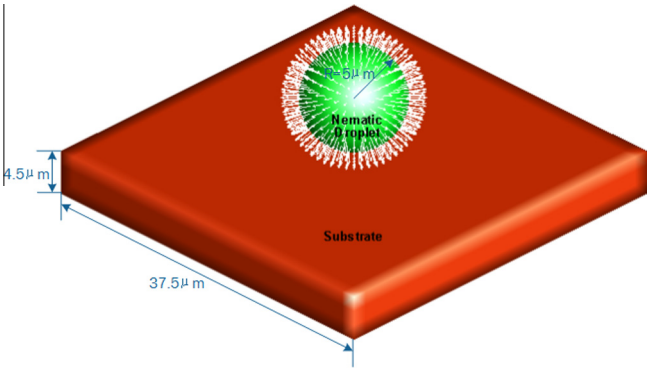

Fig. 4. Computational model of the nematic liquid crystal elastomer droplet and the elastic substrate.

4.3. Cell crawling on a stiffness-varying substrate

One of the main advantages of the liquid crystal elastomer cell model proposed here is its potential to describe acto-myosin dynamics and lamellipodium dynamics, which are the central issues of modeling cell motility and migration. It is maybe of great interest to examine cell interaction with a substrate that has non-uniform stiffness, because the non-homogeneous rigidity provides an external stimuli that may trigger contractility of the cell, and eventually leads to the typical crawling phenomena. For this purpose, a cell is placed on an extracellular matrix that has a gradient of rigidity along the y direction. In specific, the Hyperelastic constitutive parameters of the substrate is a function of y coordinate,

$$c_1 = 2.126\left(\frac{4.0y}{L_0} + 0.5\right) \times 10^3\ \text{Pa},$$
$$c_2 = 1.7\left(\frac{4.0y}{L_0} + 0.5\right) \times 10^2\ \text{Pa},$$
$$\lambda = 1.7\left(\frac{4.0y}{L_0} + 0.5\right) \times 10^5\ \text{Pa}, \tag{18}$$

where L_0 is the length of the matrix in y direction. A schematic of the problem statement is shown in Fig. 6. In Fig. 7, we display a time sequence of a cell spreading/crawling over the elastic stiffness-varying deformable substrate. For a homogeneous elastic stiffness, a cell would move approximately in the same speed in every radius direction of the cell. Based on the simulation results obtained from the inhomogeneous substrates, one may find that the cell first adheres to the substrate (see Fig. 7a–d). Then it protrudes towards the direction of higher rigidity (see Fig. 7e–h). From $t = 4.2$ μs (Fig. 7h)) to $t = 4.8$ μs (Fig. 7i)), it seems that the front part of the cell adheres to the substrate and the rear part contacts and moves towards the y direction. Compare the center of the cell at the starting point with its center at the end of the simulation ($t = 6.6$ μs), one can clearly see the cell actually moves towards the right side of the substrate. This real three dimensional simulation not only

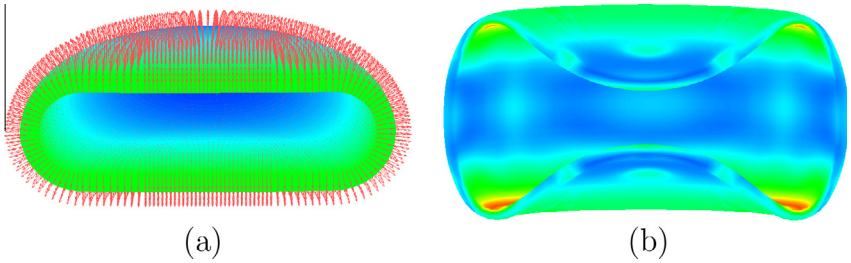

Fig. 3. (a) Initial shape for cell membrane model and (b) biconcave cell shape from simulation.

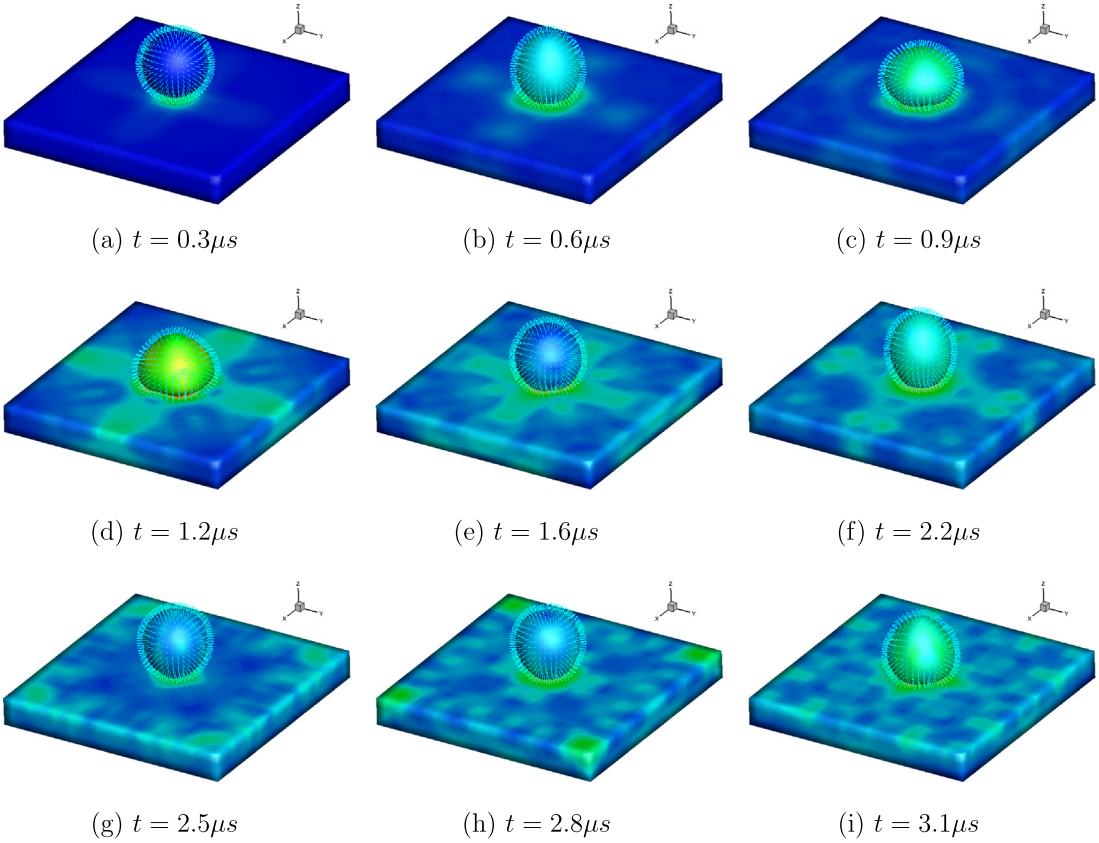

Fig. 5. Time sequence of a liquid elastomer gel in contact with an elastic substrate.

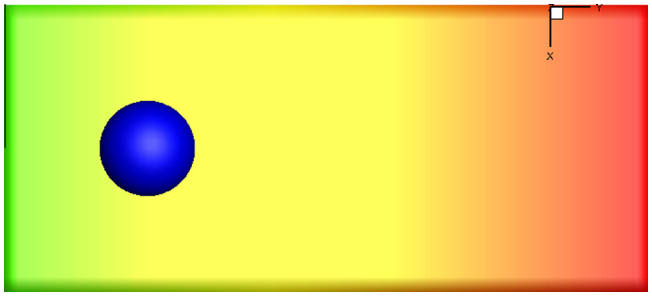

Fig. 6. 3D Computational model of cell spreading on a stiffness-varying substrate, the color in the substrate stands for different stiffness, the stiffness at the right end is the highest (top view). (For interpretation of the references to color in this figure legend, the reader is referred to the web version of this article.)

demonstrates a preliminary cell crawling and protrusion behaviors, but also indicates that the cell motility is in favor of a stiffer substrate, which is in good agreement of the experimental measurements of cell adhesion and migration reported in [5,33].

There are several crucial points for the simulation of cell crawling or motility. First, an active stress term is needed to be include in the constitutive modeling of the soft-cell model. The active stress term, $-\zeta h_i h_j$, provides contractile force that will generate internal treadmilling of the cytoskeleton polymer. It represents the stress contribution from the internal "energy pump". Second, the Coarse-Grained Contact Model, which successfully makes the cell adhere to the substrate. And third, the moving contact line formulation, which includes the surface tension effects for the three phase system based on the Gurtin–Murdoch theory, has to be included.

5. Discussions

It is of great challenge to develop a three-dimensional, computational, soft-matter based cell model, which can explain cell adhesion, crawling and its structure transformation, especially if one wants to predict real cellular motion and transformation. The proposed soft matter cell model may be viewed as a first step towards this long term goal.

In this work, an active stress based liquid crystal elastomer model is first introduced. The proposed soft matter based cell model can successfully reproduce the biconcave shape of a red blood cell membrane, which indicates that the soft-matter cell model presented here may be valid. In fact, the replication of the biconcave shape of red blood cell based on the Helfrich's liquid crystal cell membrane model [11] is regarded as the first triumph of soft matter physics.

Then a complete 3D simulation of the contact/adhesion between the proposed cell model and a hyperelastic substrate presented. It is revealed that the model proposed, combined with the CGCM, can easily be employed to cell spreading/adhesion, which is the first part of cell crawling.

After that, the present cell model successfully spreads/adheres/crawls over a non-uniform substrate. The driving force of the cell spreading/adhesion is the particle interactions between the cell and the substrates, and the crawling of the cell is mainly due to the gradient of the substrate rigidity. The author also wants to mention the importance of the surface tension effects in the simulation of the cell crawling phenomenon.

Even though we have shown that the present model may be used as a simulation tool to qualitatively study the contact and adhesion of cells to gain understanding of the information exchange between the cell and the substrate or cell signaling, it should be noted that the behaviors of cells are very complex.

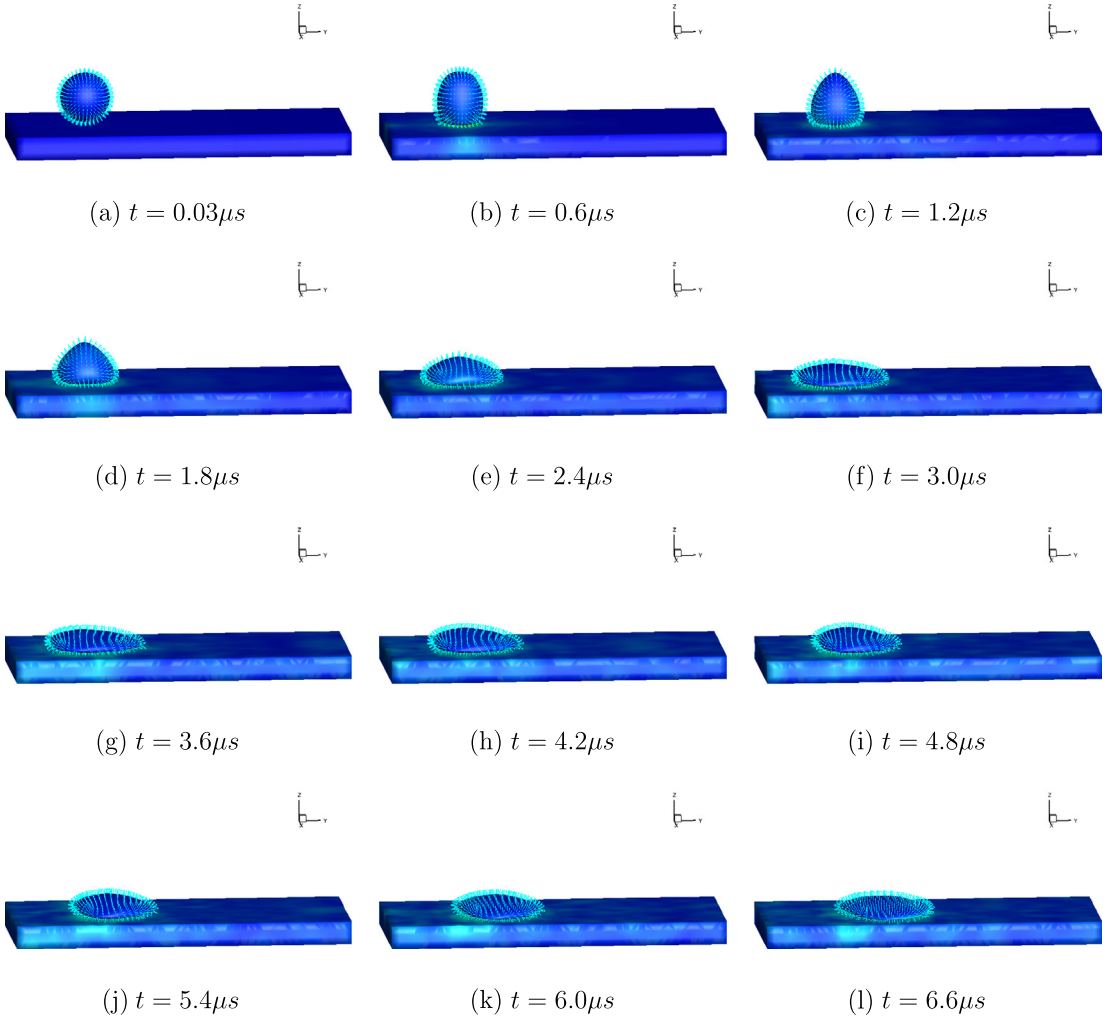

Fig. 7. Time sequence of the cell adhesion/crawling over an elastic substrate.

The proposed soft matter cell model is only intended to model mechanical behaviors of cells at a mesoscale level, which may not and cannot explain the molecular mechanisms of cellular processes such as evolution and proliferation, and to understand the molecular mechanism of the cellular process requires an in-depth study of every aspects of molecular cell biology including all relevant bio-chemical, bio-physical, as well as bio-mechanical factors and their interactions at different scales.

The soft matter cell model presented in this work is a primitive one, but it may have open a door for more realistic and more accurate modeling of cells. It is possible that along this line more sophisticated soft matter models can be developed by incorporating more features at molecular level that are capable of simulating self-assembly of focal adhesion, cell division, proliferation and more. The predictive ability of the soft matter cell model may provide both scientific insight as well as clinic guidance on many health problems, such as drug design or delivery.

Acknowledgements

This research is supported by A. Richard Newton Research Breakthrough Award from Microsoft Corporation and a grant from National Science Foundation (CMMI No. 0800744), United States. These supports are greatly appreciated. H. Fan would like to thank Chinese Scholarship Council (CSC), China, for a graduate fellowship.

References

[1] G.I. Bell, Science 200 (1978) 618–627.
[2] G.I. Bell, M. Dembo, P. Bongrand, Biophys. J. 45 (1978) 1051–1064.
[3] J.W. Cahn, S.M. Allen, J. Phys. 38 (1977) C7:51–54.
[4] S.A. Edwards, J.M. Yeomans, Eur. Lett. Phys. 85 (2009). Article No. 18008.
[5] A.J. Engler, S. Sen, H.L. Sweeney, D.E. Discher, Cell 126 (2006) 677–689.
[6] T. Frisch, O. Thoumine, J. Biomech. 35 (2002) 1137–1141.
[7] I. Fried, A.R. Johnson, Comput. Methods Appl. Mech. Eng. 69 (1988) 53–64.
[8] E. Fried, V. Korchagin, Int. J. Solids Struct. 39 (2002) 3451–4367.
[9] M.E. Gurtin, A.I. Murdoch, Arch. Rational Mech. Anal. 57 (1975) 291–323.
[10] M.E. Gurtin, A.I. Murdoch, Int. J. Solids Struct. 14 (1978) 431–440.
[11] W. Helfrich, Z. Naturforsch. C 28 (1973) 693–703.
[12] J.F. Joanny, J. Prost, HFSP J. 3 (2009) 94–104.
[13] F. Jülicher, K. Kruse, J. Prost, J.F. Joanny, Phys. Rep. 449 (2007) 3–28.
[14] K. Kruse, J.F. Joanny, F. Jülicher, J. Prost, K. Sekimoto, Eur. Phys. J. E 16 (2005) 5–16.
[15] K. Kruse, J.F. Joanny, F. Jülicher, J. Prost, Phys. Biol. 3 (2006) 130–137.
[16] S. Li, W. Kam Liu, Meshfree Particle Methods, Springer, Berlin, 2004.
[17] W.K. Liu, S. Li, T. Belytschko, Comput. Methods Appl. Mech. Eng. 143 (1997) 113–154.
[18] G. Marckmann, E. Verron, Rubber Chem. Technol. 79 (5) (2006) 835–858.
[19] H. Minaki, S. Li, Comput. Methods Appl. Mech. Eng. 273 (2014) 273–302.
[20] Y. Ni, M. Chiang, Soft Matter 3 (2007) 1285–1292.
[21] S. Roy, H. Jerry Qi, Biomech. Model. Mechanobiol. 9 (2010) 573–581.
[22] R. Sauer, S. Li, Int. J. Numer. Methods Eng. 71 (2007) 931–962.
[23] R. Sauer, S. Li, Finite Elements Anal. Des. 43 (2007) 384–396.
[24] R. Sauer, S. Li, J. Nanosci. Nanotechnol. 8 (2007) 1–17.
[25] U. Schwarz, Soft Matter 3 (2007) 263–266.
[26] F. Vernerey, M. Farsad, J. Mech. Behav. Biomed. Mater. 4 (8) (2011) 1683–1699.
[27] J. Viamontes, J.X. Tang, Phys. Rev. E 67 (2003). article no. 040701.
[28] J. Viamonte, S. Narayanan, A.R. Sandy, J.X. Tang, Phys. Rev. E 73 (2006) 061901.
[29] X.-J. Wang, Q.-F. Zhou, Liquid Crystalline Polymers, World Scientific, Singapore, 2004.

[30] M. Warner, E.M. Terentjev, Liquid Crystal Elastomers, Oxford Scientific Publication, Clarendon Press, Oxford, 2007.
[31] J.P. Winer, S. Oake, P.A. Janmey, PLoS ONE 4 (7) (2009) e6382.
[32] S.J. Woltman, G.D. Jay, G.P. Crawford, Nat.Mater. 6 (2007) 929–938.
[33] J.Y. Wong, A. Velasco, P. Rajagopalan, Q. Pham, Langmuir 19 (2003) 1908–1913.
[34] A. Zemel, F. Rehfeldt, A.E.X. Brown, D.E. Discher, S.A. Safran, Nat. Phys. 6 (2010) 468–473.
[35] X. Zeng, S. Li, J. Mech. Behav. Biomed. Mater. 4 (2011) 180–189.
[36] X. Zeng, S. Li, Comput. Methods Biomech. Biomed. Eng. 14 (2011) 447–458.
[37] X. Zeng, S. Li, Soft Matter 8 (2011) 5765–5776.